Topographic modulation on the layered circulation in South China Sea

Qibang Tang[12], Zhongya Cai[12], Zhiqiang Liu[3]

1 State Key Laboratory of Internet of Things for Smart City, Department of Ocean Science and Technology, University of Macau, China

2 Centre of Ocean Research in Hong Kong and Macau (CORE), Hong Kong, China

3. Department of Ocean Science and Engineering and Center for Complex Flows and Soft Matter Research, Southern University of Science and Technology, Shenzhen, China

Correspondence to: Zhongya Cai (zycai@um.edu.mo)

Abstract: The South China Sea (SCS) is the largest semi-enclosed marginal sea in western Pacific. It exhibits a unique vertically rotating cyclonic, anticyclonic, and cyclonic circulation in its upper, middle, and deep layers. Over slope topography, these layered currents interact and significantly shape the structure and intensity of the basin circulation. In this study, we employ process-oriented numerical simulations to investigate how upper-layer processes, characterized by greater magnitude and variability, influence the layered circulation over the irregular topographic slope. The simulations reveal that stronger upper intrusion from open ocean directly enhances upper layer circulation, which subsequently strengthens the middle and the deep slope currents. Vorticity dynamics illustrate that changes in the middle and deep slope current are largely related to the vertical stretching (ζ_DIV) induced by bottom geostrophic cross-isobath transport (CGT_b). As the upper-layer cyclonic slope current intensifies, it modulates the bottom pressure distribution, resulting in stronger negative ζ_DIV predominantly over the northwestern slope to intensify the middle anticyclone slope current. Similarly, for the deep cyclonic slope current, the CGT_b maintains downwelling in the northern part and upwelling over the southern slope. Over the southern slope, the strengthening of the positive CGT_b is induced by the increment of the advection of relative vorticity and planetary vorticity in water column, in which the middle layer has important contribution, but the upper layer has a minimal impact. Conversely, on the northern slope, the strengthening of the negative CGT_b is primarily influenced by the upper layer.

Keywords: Circulation dynamics; Layered circulation; Process-oriented simulation; Topographic modulation; Vertical coupling

1. **Introduction**

Marginal seas circulation plays crucial role in the mass transport and regional climate dynamics, with circulation patterns being strongly influenced by their unique topographic features (Millot 1999, Omstedt, Elken et al. 2004, Oey, Ezer et al. 2005, Gan, Li et al. 2006, Johns and Sofianos 2012). This topographic regulation results in intricate layered slope currents that flow in different directions at various depths (Yuan 2002, Wang, Xie et al. 2011, Lan, Zhang et al. 2013, Gan, Kung et al. 2022). These layered currents interact over slope topography, significantly shaping the structure and intensity of the overall circulation (Gan, Liu et al. 2016, Quan and Xue 2018). For instance, in the Gulf of Mexico, loop current eddies influence not just the upper-layer circulation but also the deep flow, illustrating the importance of vertical coupling in transferring energy and variability to deeper currents (Tenreiro, Candela et al. 2018). Understanding these dynamics helps elucidate the behavior of marginal sea's circulation (Liang, Spall et al. 2017, Zhu and Liang 2020, Olvera-Prado, Moreles et al. 2023).

The South China Sea (SCS) is the largest semi-enclosed marginal sea located in the tropical region. It exhibits a unique mean cyclonic, anticyclonic, and cyclonic (CAC) circulation in its upper, middle, and deep layers (Wang, Xie et al. 2011, Shu, Xue et al. 2014, Lan, Wang et al. 2015, Gan, Liu et al. 2016, Zhu, Sun et al. 2017). The strong upper layer circulation is driven by the Asia monsoon and Kuroshio intrusion from Luzon Strait (LS), while the middle and deep circulations are maintained by the outflux and deep intrusion through LS, respectively. Based on current understanding, the upper-layer influx through the Luzon Strait (LS) is induced by the Kuroshio Current as it passes through the strait (Nan et al., 2015). The middle-layer outflux and deep-layer intrusion, on the other hand, are largely driven by density differences caused by contrasting turbulent mixing intensities (e.g., Tian et al., 2009; Zhu et al., 2019; Zhou et al., 2023). Over the slope topography, the CAC circulation affects each other through the vertical coupling among them (Shu, Wang et al. 2018). For example, the study of Quan and Xue (2018) demonstrated that perturbations in the upper layer can transit through the water column and affect deeper circulation by altering layer thickness. This coupling is particularly evident over the strong boundary current that in the northern basin and along the western boundary. Numerical experiments by Wang et al. (2018) suggest that, although the basin-scale circulation is primarily driven by the LS overflow, upwelling patterns are essential in shaping the detailed structure of the deep-water circulation. Similar processes have been observed in other marginal seas as well (e.g., Testor et al., 2018; Wang et al., 2024; Xu et al., 2009; Olvera-Prado, Moreles et al. 2023).

Despite advances in understanding the major features of mean layered circulation, the response of this circulation to changes in external forcings—particularly the strong upper ocean

processes—and the specific mechanisms involved remain poorly understood. A comprehensive understanding of how topographically modulated vertical coupling over basin slopes influences the structure and intensity of mean circulation is crucial for exploring the long-term evolution of marginal sea circulation. For instance, Kuroshio intrusion has been observed to weaken with decadal variations, while upper ocean currents have shown acceleration in response to a warming climate (Peng et al., 2022; Chen et al., 2019; Nan et al., 2013). How the layered circulation in marginal seas responds to these changes remains unclear. This study employs process-oriented simulations to elucidate how upper-layer processes, which exhibit greater intensity and variability, influence layered circulation over the curved bottom slope in the SCS. The paper is organized as follows: Section 2 explains the configuration of the simulation. Section 3 offers the response of layered slope current intensity to the changes of the upper circulation. Section 4 explores the underlying physical mechanisms. Finally, Section 5 provides a summary of our findings.
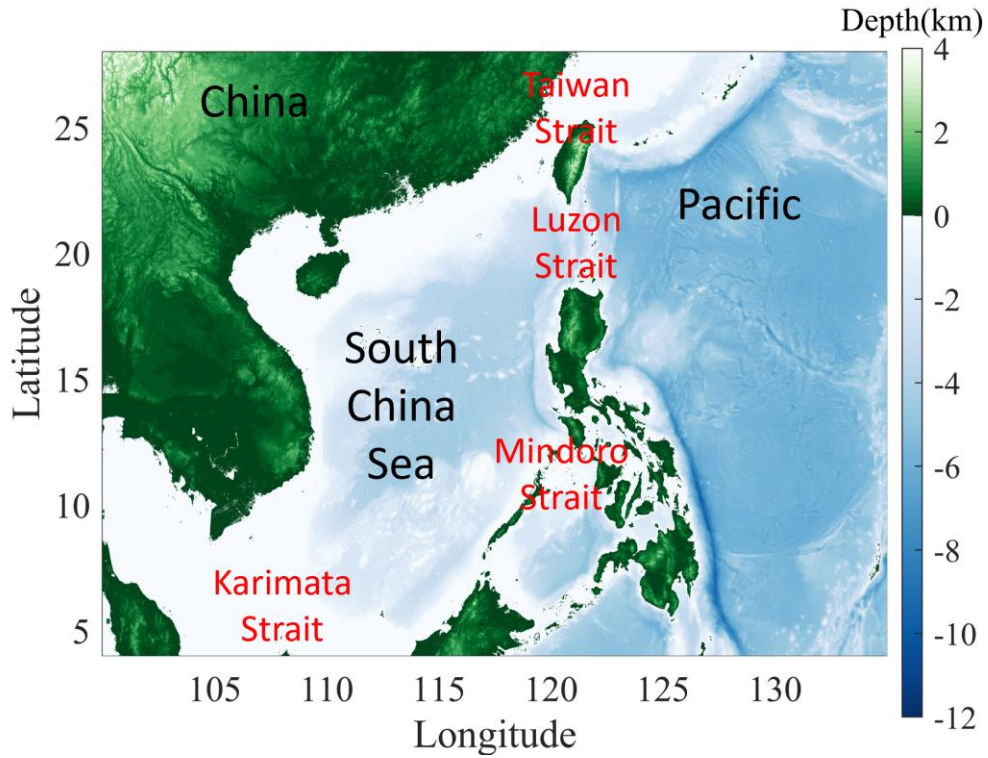
Figure1. Location and bathymetry (km) of the South China Sea, showing Luzon Strait, Taiwan Strait, Mindoro Strait, and Karimata Strait.

2. Methodology

Based on the Regional Ocean Modeling System (ROMS) (Shchepetkin & McWilliams, 2005), we performed a three-dimensional process-oriented simulation in this study (Cai et al., 2023). The model setup included a circular basin on the west representing the SCS and a

98 rectangular basin on the east representing the Western Pacific Ocean. The slope in the SCS

99 increases from 400 to 4000 m and the central basin has the depth of 4000 m. The SCS and

100 Pacific basins were connected by a narrow strait (representing the LS) with a depth of 2500 m.

101 The model employed a uniform horizontal grid with a 5 km resolution, and the vertical

102 structure utilized stretched, terrain-following coordinates with 30 layers (Song and Haidvogel

103 1994) were adopted with 30 layers. Near the surface and bottom boundaries, the vertical

104 resolution is refined with spacing of approximately 0.01. In the upper layer, an influx of 25 Sv

105 and an outflux of 20 Sv were specified at the southeastern and northeastern boundaries of the

106 open ocean, respectively (Figure 2c). The SCS was opened to the south with the depth of 400

107 m (Figure 2a), to allow the upper-layer intrusion to develop intrinsically during the simulation.

108 To simulate the density differences and exchange currents in the middle and deep layers of the

109 LS, the model incorporated variable contrasting mixing coefficients (K_v) between the SCS and

110 the Western Pacific Ocean (Tian, Yang et al. 2009, Yang, Zhao et al. 2016). In the SCS and the

111 western half of the LS, K_v values were set as $5 \cdot 10^{-4} m^2 s^{-1}$ between 500 and 1,500 m, $2 \cdot$

112 $10^{-3} m^2 s^{-1}$ below 1,500 m, and $5 \cdot 10^{-3} m^2 s^{-1}$ in the layer 500 m from the bottom. In the upper

113 500 m of SCS and LS, and throughout the entire water column of the open ocean, a background

114 K_v of $2 \cdot 10^{-5} m^2 s^{-1}$ was applied. The K_v was designed based on observational work by Yang

115 et al. (2016) and estimations by Wang et al. (2017) to form the circulation in the semi-enclosed

116 middle and deep layers. Then, simulations were conducted to explore the response of the

117 layered slope current, particularly in the semi-enclosed middle and deep layers, to changes in

118 the upper-layer circulation. A zonal wind stress with meridional variations was applied over

119 the open ocean, while the atmospheric buoyancy flux over the SCS was simplified by setting it

120 to zero. This model simplifies the configurations to focus on the fundamental dynamics of the

121 system. While these simplifications are essential for isolating key mechanisms, they may not

122 capture the complexity of real-world conditions, potentially limiting its quantitative

123 applicability to realistic processes.

124 The model was initialized with horizontally uniform temperature and salinity profiles

125 derived from the mean data of the World Ocean Atlas, averaged over the region west of the LS.

126 The simulation ran for 25 years, with the analysis was conducted on the results from the final

127 5 years average after the layered circulation reached a stable state.

128

129
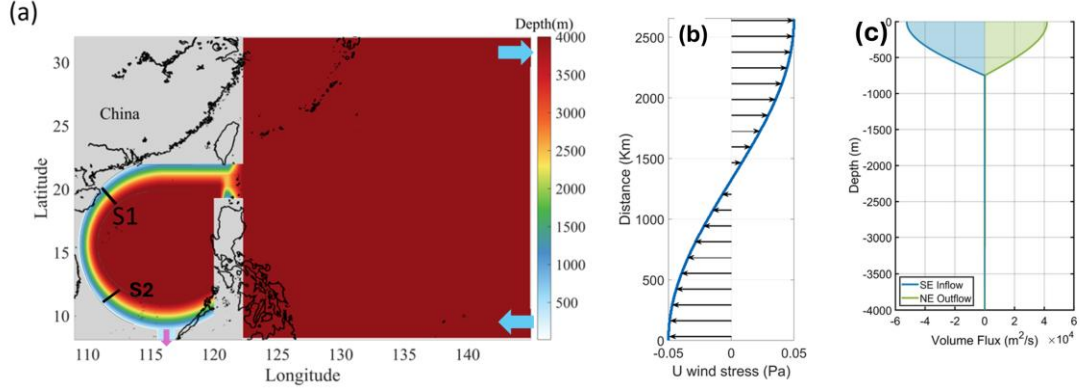
Figure 2. (a) The topography and geometry used in the idealized process-oriented simulation. The black lines show the realistic surrounding coastline. S1 and S2 are two vertical sections for showing slope current. (b) Distribution of the wind stress. (c) Vertical profile of the volume inflow/outflux (m^2/s) through the southern/northern part of the eastern boundary

3. Results

In the LS, the influx occurs in the upper and deep layers, while the outflux occurs in the middle layer between them (Figure 3b). The upper intrusion is intrinsically linked to the western boundary current in the open ocean, i.e. Kuroshio Current. In the middle and bottom layers, the exchange currents are primarily related to the density differences between the South China Sea (SCS) and the Pacific. Although the initial temperature and salinity distributions are horizontally uniform, the intensified turbulent mixing within the deep SCS basin gradually leads to a density difference between the two sides of the LS. Specifically, the deep SCS exhibits lower density compared to the Pacific basin (Figure S1). Under the density difference, the westward pressure gradient was formed that drives the deep intrusion from the open ocean towards the SCS. Those features are consistent with established understandings from previous studies (e.g., Wang, Xie et al. 2011, Zhu et al., 2017, 2019; Cai, Chen et al. 2023; Zhou et al., 2023). Associated with the simulated layered exchanging current, the layered circulations developed inside the SCS basin. The upper, middle, and deep layers exhibit circulation in cyclonic, anticyclonic, and cyclonic directions, respectively (Figure S1). The horizontally averaged vorticity features with the positive-negative-positive values in the respective depth of the basin (Figure 3b).
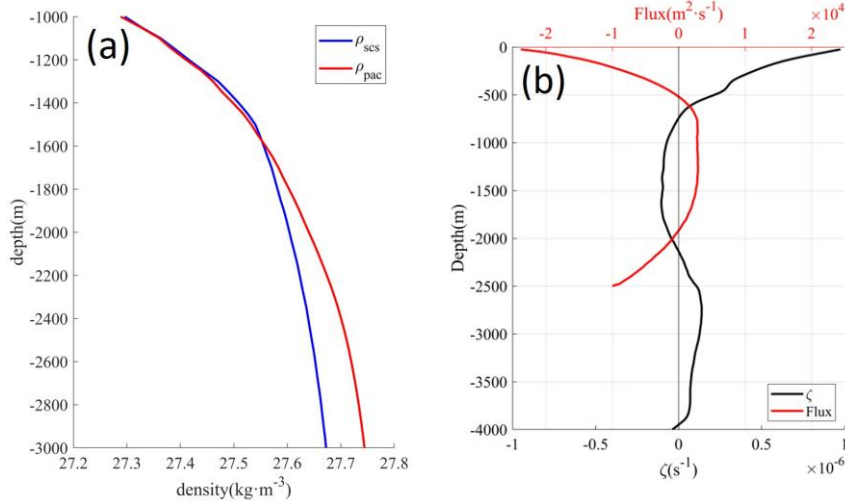
Figure 3. (a) Vertical profile of domain averaged density ρ (kg·m⁻³) in SCS and Pacific between 1000m to 3000m. (b) Black line shows the vertical profile of the SCS basin-averaged vorticity (s⁻¹) and the red line shows the flux through LS (m²·s⁻¹). The positive/negative vorticity represents the cyclonic/anticyclonic circulation, and the positive/negative value flux represents the outflux/influx through LS.

To investigate how the changes in upper layer current modulates the layered circulation, additional numerical experiments were conducted by adjusting the northeastern outflux to 22Sv, 23Sv and 24Sv, thus the upper LS intrusion was adjusted to 3Sv (Case_U3), 2Sv (Case_U2) and 1Sv (Case_U1). In these scenarios, the middle and deep exchanging currents, which were primarily sustained by the contrasting densities between the SCS and the open ocean, remained relatively unchanged (Figure 4a). Inside the basin, the enhancement of the upper layer inflow directly intensified the upper layer cyclonic circulation (Figure 4 c-f). And subsequently strengthened the middle anticyclonic slope current, particularly in the northwestern part of the basin (transect S1, Figure 4c, d). Additionally, although not directly connected to the upper layer, the deep cyclonic slope current also exhibited increased strength (Figure 4c-f). Using the domain-averaged vorticity as an indicator, it was observed that the intensification of the upper layer circulation resulted in a 10% increase in the intensity of the middle anticyclonic circulation and a 27% increase in the deep cyclonic circulation (Figure 4b). Given that only the upper layer circulation is directly amplified by the upper intrusion, the remote influence from upper layer processes over the basin slope significantly impacts the intensity of the layered circulation, which was explored below.

177

178

179
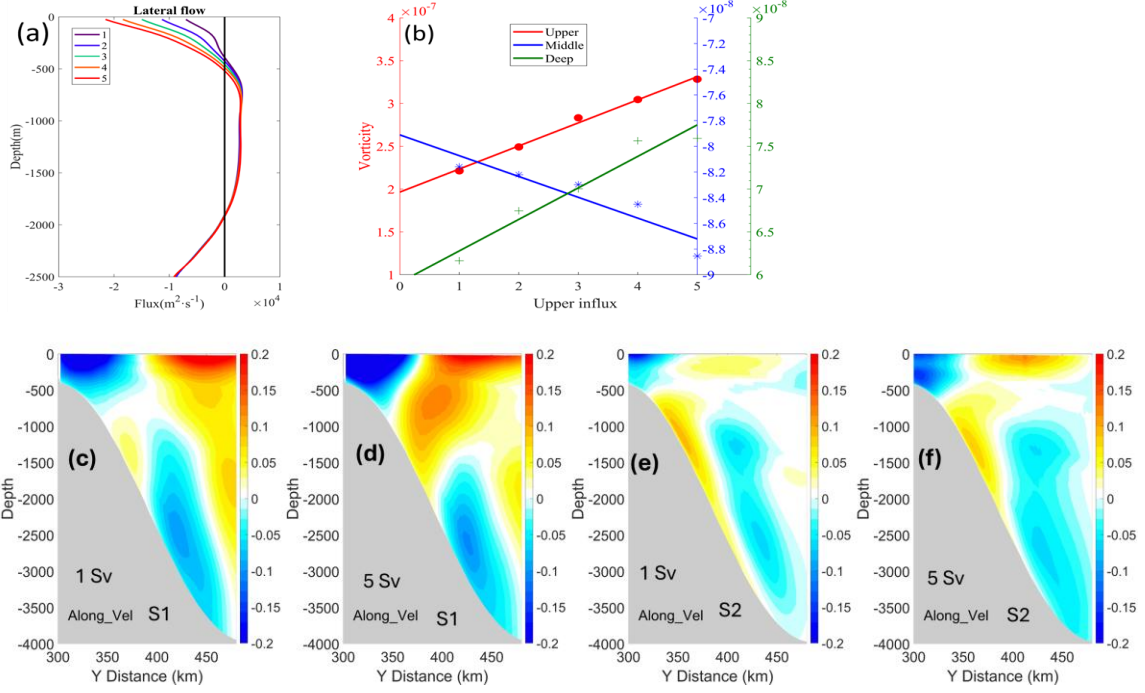
Figure 4. (a) Vertical profile flux across the LS under varying upper layer influx. (b) Changes
in the basin-averaged vorticity between 0-500 m (Upper), 1000-2000 m (Middle) and 3000-
4000 m (Deep) with different upper influx. (c-f) The along-slope current $(m \cdot s^{-1})$ over the
section S1 and S1 in Standard case (upper intrusion is 5 Sv) and Case_U1 (upper LS intrusion
is 1Sv), respectively. The locations of the two transects are shown in Figure 1a. The transect
locations are indicated in Figure 1a. Positive values represent anticyclonic flow, while negative
values indicate cyclonic flow.

4. Discussion

To understand how the upper layer processes modulate the layered current over the slope,
we first investigated the layered-integrated vorticity budget for each layer (Gan, Liu et al. 2016,
Cai, Chen et al. 2023):

$$\overbrace{\int_A [\nabla \times \int_{H_1}^{H_2} (\overrightarrow{PGF})\, dz]\, dA}^{\zeta\_PGF} + \overbrace{\int_A [\nabla \times \int_{H_1}^{H_2} (\overrightarrow{ADV})\, dz]\, dA}^{\zeta\_ADV} + \overbrace{\underbrace{\int_A \left[-f\nabla \cdot \int_{H_1}^{H_2} (\overrightarrow{V}_h)\, dz \right]\, dA}_{\zeta\_DIV} + \underbrace{\int_A \left[-\beta \cdot \int_{H_1}^{H_2} (v)\, dz \right]\, dA}_{\zeta\_BETA}}^{\zeta\_COR} +$$

$$\overbrace{\int_A [\nabla \times \int_{H_1}^{H_2} (\overrightarrow{VIS})\, dz]\, dA}^{\zeta\_VIS} = 0 \quad (1)$$

where $\overrightarrow{PGF}$ is pressure gradient force, $\overrightarrow{ADV}$ is nonlinear advection, $\overrightarrow{VIS}$ is the turbulent
viscosity. The horizontal viscosity is much smaller than vertical viscosity term and they are
included in the $\overrightarrow{VIS}$ term for simplicity. COR is the Coriolis force and the domain-integrated
ζ_COR represents the lateral planetary vorticity flux. The H_1 and H_2 represent the bottom and
upper depth of each layer, respectively. Inside the basin, the ζ_COR can be further decomposed
into the vertical stretching induced by the divergence of the horizontal flow (ζ_DIV) and β

202 effect of the meridional current (ζ_BETA).

203   The circulation in SCS is primarily governed by geostrophic balance, manifested as
204 ζ_COR balanced by the ζ_PGF in both layers. It suggests that the mean cyclonic/anticyclonic
205 circulation is related to the lateral planetary vorticity influx/outflux (Figure 5) (Cai and Gan
206 2019, Cai, Chen et al. 2023; Zhu et al., 2017, 2019). Consequently, the strengthening of the
207 upper LS intrusion directly intensifies the upper layer cyclonic slope current by providing more
208 positive planetary vorticity flux. In the semi-enclosed middle and deep layers, the vorticity
209 input is mainly provided by the ζ_DIV, as also highlighted in the previous studies (Zhu, Sun et
210 al. 2017, Wang, Du et al. 2018, Cai, Chen et al. 2023). The positive ζ_DIV in the upper and
211 deep layers reflects the downward and upward flux, which squeeze the middle layer and provide
212 the negative vertical flux (negative ζ_DIV) for the anticyclonic circulation. Therefore, the
213 intensification of the middle and deep slope currents is largely attributed to vertical stretching
214 over the basin slope.

215

216
217
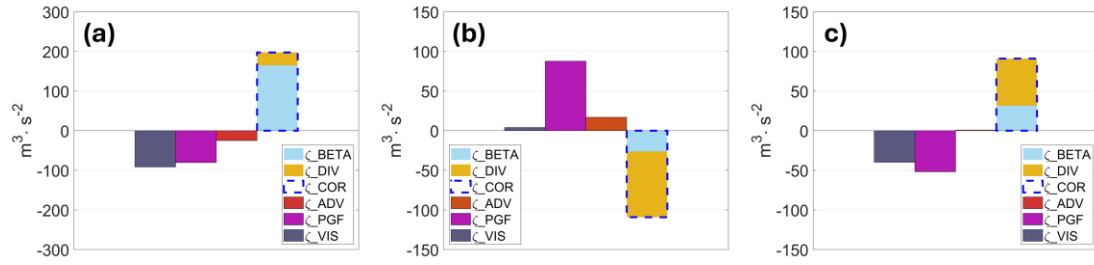
218 **Figure 5.** The layered-integrated vorticity budget (Equation 1) for the standard case in the layers of (a)
219 0–500, (b) 1,000–2,000, and (c) 2,500–4,000 m.
220

221

a. Intensification of middle anticyclonic slope current

223

224 For the middle anticyclonic slope current, the negative middle-layered ζ_DIV (ζ_DIV_M) mainly
225 occurs over the northwestern slope (Figure 6a), where a relatively strong anticyclonic slope
226 current is observed. In this area, the upper layer generally exhibits positive ζ_DIV (ζ_DIV_U),
227 indicating downward squeezing from the upper layer that helps maintain the middle
228 anticyclonic slope current (Figure 6 b). The increased squeezing from the upper slope current
229 is expected to intensify the middle anticyclonic slope current (Figure 4 c, d). Since the
230 stretching/squeezing imposed on the slope current is closely related to the vertical motion
231 (Liang, Spall et al. 2017), the mean vertical motions over the slope can be understood as follows:

232 $$\bar{w} = -\nabla_h \cdot \int_{-H}^{z} \bar{\vec{V}}_h dz \approx -\nabla_h \cdot \int_{-H}^{z} \bar{\vec{V}}_{h\_geo} dz - \nabla_h \cdot \int_{-H}^{z} \bar{\vec{V}}_{h\_vis} dz$$

233 $$=\overbrace{-(\bar{v}_{b\_geo}H_y+\bar{u}_{b\_geo}H_x)}^{CGT_b}+\underbrace{\frac{\beta}{f}\int_{-H}^{z}\bar{v}_{geo}dz}_{\beta\,effect}-\overbrace{\nabla_h\cdot\int_{-H}^{z}\vec{\bar{V}}_{h\_vis}dz}^{Fric}\quad(2)$$

234 where H is the topography, $\_geo$ represents the geostrophic component of the horizontal

235 current, which is maintained by the distribution of bottom pressure. $\_vis$ represent the vertical

236 viscosity component. H_x and H_y are the horizontal gradients of the bottom slope, $\bar{u}_{b\_geo}$ and

237 $\bar{v}_{b\_geo}$ are the bottom geostrophic currents. When the current flows over the slope, the bottom

238 pressure distribution interacts with the curved topography and the resulting geostrophic cross-

239 isobath transport (CGT_b) to influence the vertical motions over the slope. The *Fric* represent

240 the effect of the bottom Ekman pumping that induced by the bottom stress of the slope current.

241 Generally, the CGT_b largely governs the mean vertical motion over northwestern slope, which

242 in turn squeezes and stretches the middle and upper slope currents. This process is crucial in

243 maintaining the vorticity input through ζ_DIV (Figure 6 d), thereby sustaining the dynamics of

244 the slope currents.

245   Associated with the intensification of the upper layer cyclonic slope current, the stronger

246 slope current modulates the bottom pressure distribution over the slope, leading to stronger

247 vertical squeezing (ζ_DIV) within the water column. The increase in squeezing gradually

248 deepens the isopycnal surface and strengthens the middle anticyclonic slope current (Figure 6e).

249
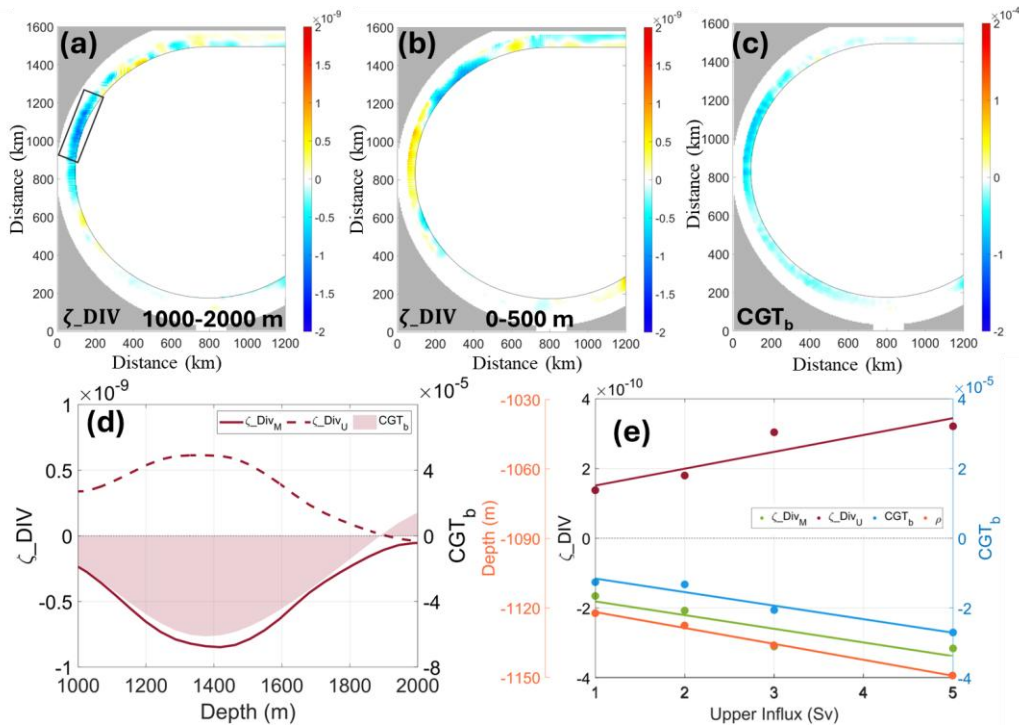
251 **Figure 6**. (a-c) ζ_DIV integrated between 1000-2000 m ($ζ\_DIV_M$), 0-500 m ($ζ\_DIV_U$), and

252 CGT_b over the region of middle anticyclonic slope current between 1000-2000 m. The black

253 line indicates the 2000 m isobath line. (d) Change of the ζ_DIV integrated between 100-2000 m

254   (ζ_DIV_M), between 0-500 m (ζ_DIV_U) with the depth over the northwestern slope. (e) Changes
255   of the ζ_DIV_M, ζ_DIV_U, CGT_b and the depth of isopycnal surface of 1027.4 kg/m^3 with different
256   upper LS influx. (d) and (e) was plotted using the data averaged over the region of black box
257   in (a)
258

259

260   **b. Intensification of the deep cyclonic slope current**

261   For the deep cyclonic slope current, the deep ζ_DIV (ζ_DIV_D) features a downward flux

262   (negative value) over the northern slope and upward flux (positive value) over the southern part

263   (Figure 7a, d). It suggests the sinking from the northern basin and upwelling from the southern

264   basin would sustain the abyssal cyclonic circulation. Same as the middle anticyclonic slope

265   current, the ζ_DIV_D is. For the deep layer, the viscosity term has an important effect in the

266   vorticity budget (Figure 5c). Similarly, the $Fric_D$ term contributes to the deep ζ_DIV_D and is

267   characterized by a relatively uniform downward motion (Figure 7d). However, the primary

268   pattern and magnitude of the ζ_DIV_D are largely controlled by the CGT_b that the pressure

269   distribution maintained the mean downwelling in the northern side and the upwelling over the

270   southern slope (Figure 7b, d). Since the $Fric_D$ is induced by the bottom frictional stress as

271   response to the deep layer slope current, while the bottom pressure is modulated by the motions

272   of water in the entire water column above it, we further examine the maintenance of the bottom

273   pressure over the slope.

274   To explain the maintenance of the bottom pressure distribution, the vertical integrated

275   vorticity dynamic was employed (Gan, Liang et al. 2013, Cai and Gan 2021):

276
$$\overbrace{\nabla \times \int_{-H}^{0} (\overrightarrow{PGF})\, dz}^{\Omega\_PGF} + \overbrace{\nabla \times \int_{-H}^{0} (\overrightarrow{ADV})\, dz}^{\Omega\_ADV} + \underbrace{\beta \int_{-H}^{0} v\, dz}_{\Omega\_BETA} - \overbrace{\nabla \times \int_{-H}^{0} (\overrightarrow{VIS})\, dz}^{\Omega\_VIS} = 0 \tag{3}$$

277   Where $\Omega\_PGF = \nabla \times \int_{-H}^{0} (\overrightarrow{PGF})\, dz = -(\bar{v}_{b\_geo}H_y + \bar{u}_{b\_geo}H_x)$, thus represents the effect of CGT_b.

278   It illustrates that the bottom pressure distribution is maintained by the nonlinear advection of

279   relative vorticity (Ω_ADV), advection of planetary vorticity (Ω_BETA), and net viscosity of the

280   current flowing over the slope topography. Among them, the Ω_BETA and Ω_ADV play the

281   major role in sustaining the bottom pressure distribution of the deep cyclonic slope current

282   (Figure 8 c, d).

283
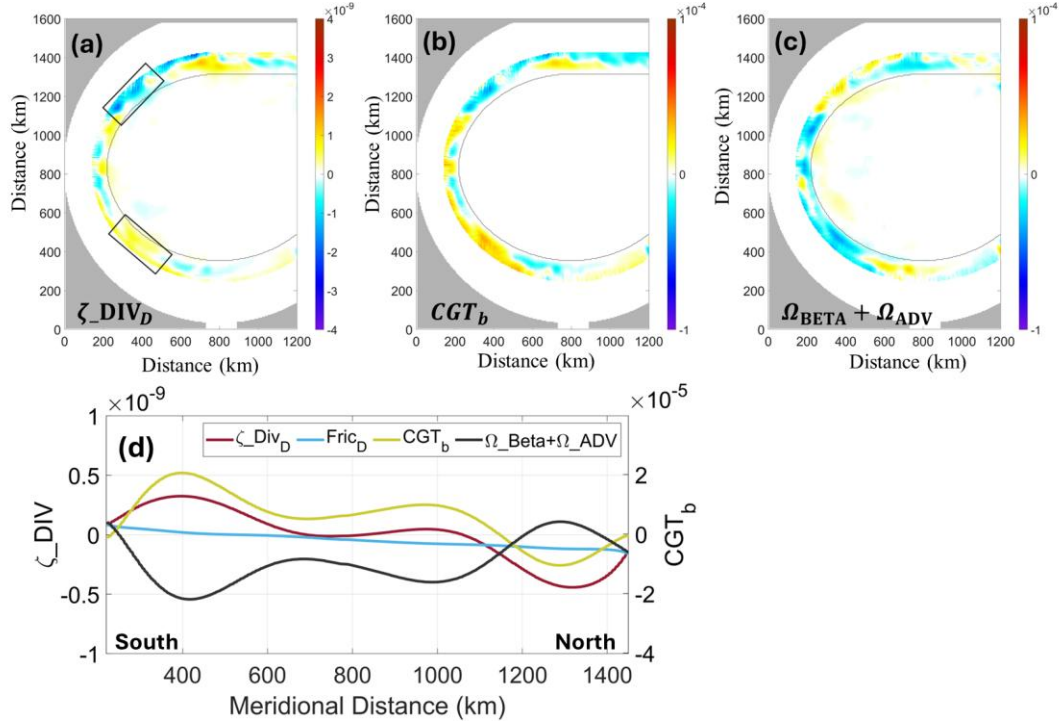
Figure 7 (a-c) ζ_DIV integrated below 3000 m of the deep cyclonic slope current (ζ_DIV$_D$), CGT_b and Ω_BETA + Ω_ADV over the region of middle anticyclonic slope current below 3000 m. The black line indicates the 4000 m isobath line. (d) Meridional changes of the ζ_DIV$_D$, Fric$_D$, CGT_b and Ω_BETA + Ω_ADV over the slope.

As the upper intrusion intensifies, the bottom pressure distribution adjusts in response to changes in the layered circulation, resulting in a gradual strengthening of the negative CGT_b over the northern slope and positive CGT_b over the southern part (Figure 8 a-b). Over the southern slope (Figure 8a), the strengthening of the positive CGT_b is induced by the increase of the Ω_BETA + Ω_ADV in the water column, in which the middle layer [Ω_BETA + Ω_ADV (M)] provides approximately 40% of the total strengthening trend, while the upper layer [Ω_BETA + Ω_ADV (U)] has a negligible impact. Conversely, over the northern slope, the strengthening of the Ω_BETA + Ω_ADV is primarily influenced by the upper layer, with the middle layer has the negative effect (Figure 8b). Thus, the intensification of downward CGT_b over the northern slope is directly modulated by the strengthening of the upper cyclonic slope current, while the intensification of upward CGT_b over the southern slope is mainly driven by the strengthening of the middle anticyclonic slope current. These changes in CGT_b enhance deep stretching, thereby strengthening the deep cyclonic slope current accordingly (Figure 8c).

304

305

306
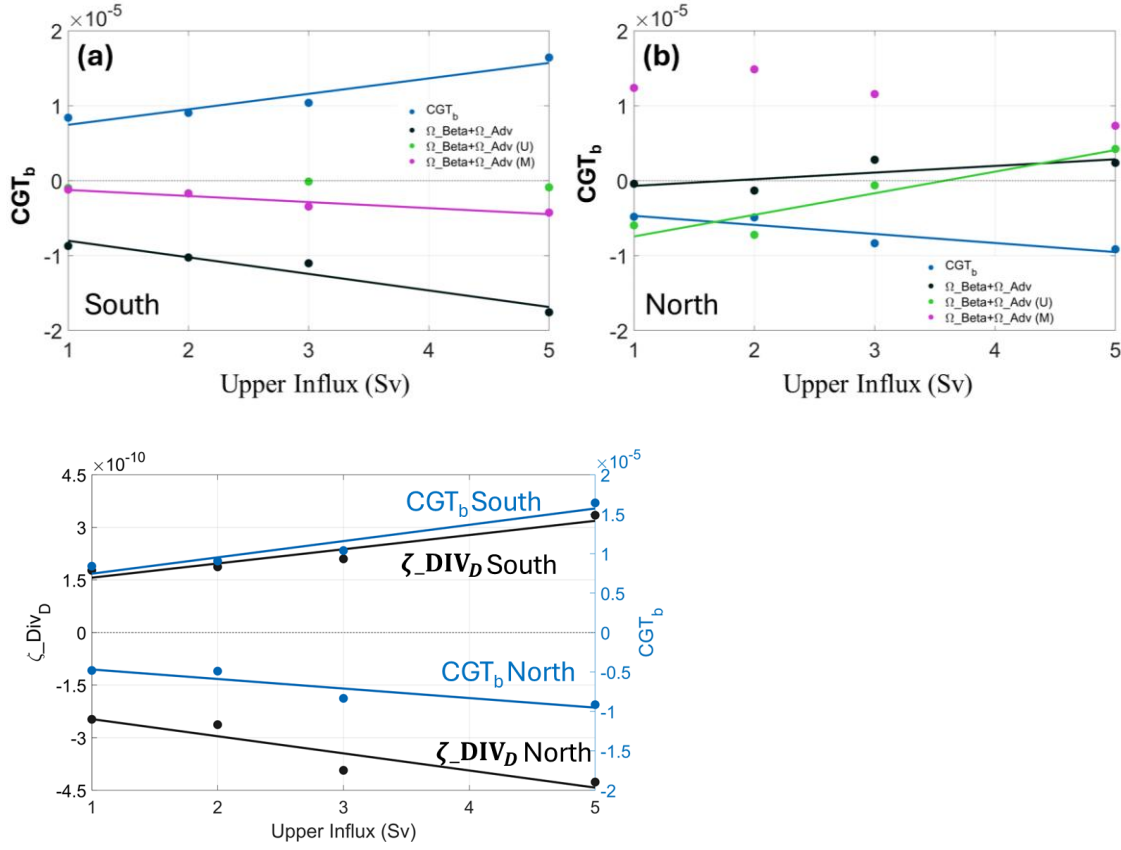
307 **Figure 8**. (a) Changes of the CGT_b, $\Omega_{Beta} + \Omega_{Adv}$ in the total water column, $\Omega_{Beta} + \Omega_{Adv}$ in the
308 layer between 0-500 m ($\Omega_{Beta\_U} + \Omega_{Adv\_U}$), $\Omega_{Beta} + \Omega_{Adv}$ in the between 1000-2000 m
309 ($\Omega_{Beta\_M} + \Omega_{Adv\_M}$) over the southern slope (black box in Figure 8a). (b) same as (a) but over
310 the northern slope (black box in Figure 8a). (c) Change of the CGT_b and ζ_DIV_D over the
311 northern and southern slope.

312

313

5. Summary

315   Marginal sea circulation plays a crucial role in mass transport and regional climate

316 dynamics. Through process-oriented numerical simulations, we examined how upper-layer

317 processes, which are characterized by greater intensity and variability, impact the layered

318 circulation over the curved bottom slope in SCS. The primary goal of our study is to provide

319 theoretical insights into the mechanisms driving layered circulation and their response to

320 changes in upper-layer motions. The results underscore the intricate balance between

321 topographical features and oceanic circulation. These insights have broad applicability to

322 understanding similar processes and phenomena in other regions, and help to predict the

323 behavior of marginal sea circulation under varying forcings conditions.

324   The numerical experiments show that the simulated layered exchange currents through the

325 LS introduce lateral planetary vorticity flux and facilitate the development of a layered basin

circulation within the SCS. Inside the basin, the intensification of upper-layer inflow directly enhances the upper-layer cyclonic circulation, which in turn strengthens the middle anticyclonic slope current, particularly in the northwestern part of the basin. Furthermore, even though the deep cyclonic slope current is not directly connected to the upper layer, it also exhibits increased strength. Using domain-averaged vorticity as an indicator, it was found that the intensification of the upper-layer circulation resulted in the increase in the intensity of the middle anticyclonic circulation and deep cyclonic circulation.

The vorticity dynamics illustrate that the changes in the middle and deep slope current is largely related to the vertical stretching over the slope (ζ_DIV). When the current flows over the slope, the bottom pressure distribution interacts with the curved topography and the resulting geostrophic cross-isobath transport (CGT_b) influences the vertical motions. For the middle anticyclonic slope current, the negative middle ζ_DIV predominantly occurs over the northwestern slope, where a relatively strong anticyclonic slope current is present. As the upper-layer cyclonic slope current intensifies, it modulates the bottom pressure distribution over the slope, providing stronger vertical squeezing ζ_DIV within the water column, which gradually strengthens the middle anticyclonic slope current. For the deep cyclonic slope current, the deep ζ_DIV is also largely controlled by the CGT_b over the slope, with the pressure distribution maintaining downwelling flows in the northern part and upwelling over the southern slope. Over the southern slope, the strengthening of the positive CGT_b is induced by the increase of the nonlinear advection of relative vorticity and planetary vorticity in the entire water column, in which the middle layer provides approximately 40% of the total strengthening trend, while the upper layer has a negligible impact. Conversely, on the northern slope, the strengthening of the negative CGT_b is primarily influenced by the upper layer, with the middle layer has the negative effect. The results from this process-oriented study deepen understanding of the intricate balance between topographical features and layered circulation, which help to improve the predictions of the long-term behavior of marginal sea circulation under varying climatic conditions. It should be noted that those understandings are based on process-oriented simulation with simplified configurations. In the following analysis, a more realistic simulation will provide more quantitative insights into the topographic modulation on the layered circulation in the marginal seas. In addition to the processes revealed in this study, other mechanisms, such as the Neptune Effect involving the eddy-slope interaction (e.g., Holloway, 1987, Stewart et al., 2024), may also play a role in influencing circulation dynamics in marginal seas like the SCS. It will be incorporated into our future investigations to improve understanding.

362 Data availability. All data used in this paper are available at

363 https://doi.org/10.5281/zenodo.13835538. The source code can be obtained upon request from

364 the corresponding author.

365

366 Author contributions. QT conducted the investigation, developed the methodology, and carried

367 out the writing (original draft preparation). ZC was responsible for the conceptualization,

368 supervision, and writing (review and editing). ZL was responsible for the conceptualization and

369 writing (review and editing).

370

371 Competing interests. The contact author has declared that none of the authors has any

372 competing interests.

373

374

375 *Acknowledgement*

376   This work was supported by National Natural Science Foundation of China

377 (42376024, 42276004), the Science and Technology Development Fund, Macau SAR

378 (File/Project no. 001/2024/SKL), and The Center for Ocean Research in Hong Kong

379 and Macau (CORE, EF014/FST-CZY/2023/HKUST). The work described in this paper

380 was substantially supported by a grant from the Research Grants Council of the Hong

381 Kong Special Administrative Region, China (AoE/P-601/23-N). CORE is a joint

382 research centre for ocean research between Laoshan Laboratory and HKUST. This

383 work was performed in part at the SICC, which is supported by the SKL-IOTSC,

384 University of Macau.

385
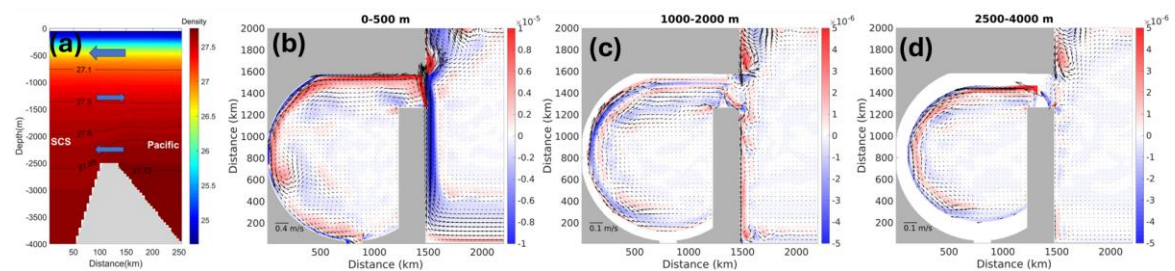
387 Figure S1. (a) Vertical transect of density (represented by color shading and contour lines)

388 across the Luzon Strait. The left side represents the SCS basin, while the right side corresponds

389 to the Pacific basin. Schematic arrows indicate the direction of the exchange flow between the

390 two basins. (b-c) The horizontal circulation (arrows) and depth averaged vorticity (color) of (b)

391 upper layer 0-500 m, (c) middle layer 1000-2000 m and (d) deep layer 2500-4000 m in the

392 standard case.

393

Reference

394

395 Cai, Z., D. Chen and J. Gan (2023). "Formation of the Layered Circulation in South China Sea With the Mixing

396 Stimulated Exchanging Current Through Luzon Strait." Journal of Geophysical Research: Oceans **128**(3).

397 Cai, Z. and J. Gan (2019). "Coupled External-Internal Dynamics of Layered Circulation in the South China Sea: A

398 Modeling Study." Journal of Geophysical Research: Oceans **124**(7): 5039-5053.

399 Cai, Z. and J. Gan (2021). "Dynamics of the Layered Circulation Inferred from Kinetic Energy Pathway in the South

400 China Sea." Journal of Physical Oceanography **51**(5): 1671-1685.

401 Gan, J., H. Kung, Z. Cai, Z. Liu, C. Hui and J. Li (2022). "Hotspots of the stokes rotating circulation in a large

402 marginal sea." Nat Commun **13**(1): 2223.

403 Gan, J., H. Li, E. N. Curchitser and D. B. Haidvogel (2006). "Modeling South China Sea circulation: Response to

404 seasonal forcing regimes." Journal of Geophysical Research **111**(C6).

405 Gan, J., L. Liang and H. San Ho (2013). "Dynamics of Intensified Downwelling Circulation over a Widened Shelf

406 in the Northeastern South China Sea." Journal of Physical Oceanography **43**(1): 80-94.

407 Gan, J., Z. Liu and C. R. Hui (2016a). "A Three-Layer Alternating Spinning Circulation in the South China Sea."

408 Journal of Physical Oceanography **46**(8): 2309-2315.

409 Gan, J., Z. Liu, and L. Liang, Numerical modeling of intrinsically and extrinsically forced seasonal circulation in the

410 China Seas: A kinematic study. Journal of Geophysical Research: Oceans, 2016b. 121(7): p. 4697-4715.

411 Holloway (1987): Systematic forcing of large-scale geophysical flows by eddy-topography interaction, Journal of

412 Fluid Mechanics.

413 Johns, W. E. and S. S. Sofianos (2012). "Atmospherically Forced Exchange through the Bab el Mandeb Strait."

414 Journal of Physical Oceanography **42**(7): 1143-1157.

415 Lan, J., Y. Wang, F. Cui and N. Zhang (2015). "Seasonal variation in the South China Sea deep circulation." Journal

416 of Geophysical Research: Oceans **120**(3): 1682-1690.

417 Lan, J., N. Zhang and Y. Wang (2013). "On the dynamics of the South China Sea deep circulation." Journal of

418 Geophysical Research: Oceans **118**(3): 1206-1210.

419 Liang, X., M. Spall and C. Wunsch (2017). "Global Ocean Vertical Velocity From a Dynamically Consistent Ocean

420 State Estimate." Journal of Geophysical Research: Oceans **122**(10): 8208-8224.

421 Millot, C. (1999). "Circulation in the western Mediterranean Sea." Journal of Marine Systems **20**(1-4): 423-442.

422 Nan, F., Xue, H. and Yu, F., 2015. Kuroshio intrusion into the South China Sea: A review. Progress in Oceanography,

423 137, pp.314-333.

424 Oey, L., T. Ezer and H. Lee (2005). "Loop Current, rings and related circulation in the Gulf of Mexico: A review of

425 numerical models and future challenges." Geophysical Monograph-American Geophysical Union **161**: 31.

426 Olvera-Prado, E. R., E. Moreles, J. Zavala-Hidalgo and R. Romero-Centeno (2023). "Upper–Lower Layer Coupling

427 of Recurrent Circulation Patterns in the Gulf of Mexico." Journal of Physical Oceanography **53**(2): 533-550.

428 Omstedt, A., J. Elken, A. Lehmann and J. Piechura (2004). "Knowledge of the Baltic Sea physics gained during the

429 BALTEX and related programmes." Progress in Oceanography **63**(1-2): 1-28.

430 Quan, Q. and H. Xue (2018). "Layered model and insights into the vertical coupling of the South China Sea

431 circulation in the upper and middle layers." Ocean Modelling **129**: 75-92.

432 Shchepetkin, A. F. and J. C. McWilliams (2005). "The regional oceanic modeling system (ROMS): a split-explicit,

433 free-surface, topography-following-coordinate oceanic model." Ocean Modelling **9**(4): 347-404.

434 Shu, Y., Q. Wang and T. Zu (2018). "Progress on shelf and slope circulation in the northern South China Sea."

435 Science China Earth Sciences **61**(5): 560-571.

436 Shu, Y., H. Xue, D. Wang, F. Chai, Q. Xie, J. Yao and J. Xiao (2014). "Meridional overturning circulation in the

437 South China Sea envisioned from the high-resolution global reanalysis data GLBa0.08." Journal of Geophysical

438 Research: Oceans **119**(5): 3012-3028.

439 Song, Y. and D. Haidvogel (1994). "A semi-implicit ocean circulation model using a generalized topography-

440 following coordinate system." Journal of Computational Physics **115**(1): 228-244.

441 Stewart et al. (2024): Formation of eastern boundary undercurrents via mesoscale eddy rectification, Journal of

442 Physical Oceanography.

443 Tenreiro, M., J. Candela, E. P. Sanz, J. Sheinbaum and J. Ochoa (2018). "Near-Surface and Deep Circulation

444 Coupling in the Western Gulf of Mexico." Journal of Physical Oceanography **48**(1): 145-161.

445 Tian, J., Q. Yang and W. Zhao (2009). "Enhanced diapycnal mixing in the South China Sea." Journal of Physical

446 Oceanography **39**(12): 3191-3203.

447 Wang, A., Y. Du, S. Peng, K. Liu and R. X. Huang (2018). "Deep water characteristics and circulation in the South

448 China Sea." Deep Sea Research Part I: Oceanographic Research Papers **134**: 55-63.

449 Wang, G., S.-P. Xie, T. Qu and R. X. Huang (2011). "Deep South China Sea circulation." Geophysical Research

450 Letters **38**(5): n/a-n/a.

451 Yabal, H. (1983). Continental margin geology, Petroleum Industry Press.

452 Yang, Q., W. Zhao, X. Liang and J. Tian (2016). "Three-Dimensional Distribution of Turbulent Mixing in the South

453   China Sea." Journal of Physical Oceanography **46**(3): 769-788.

454   Ye, R., C. Zhou, W. Zhao, J. Tian, Q. Yang, X. Huang, Z. Zhang and X. Zhao (2019). "Variability in the Deep

455   Overflow through the Heng-Chun Ridge of the Luzon Strait." Journal of Physical Oceanography **49**(3): 811-825.

456   Zhang, Z., W. Zhao, J. Tian, Q. Yang and T. Qu (2015). "Spatial structure and temporal variability of the zonal flow

457   in the L uzon S trait." Journal of Geophysical Research: Oceans **120**(2): 759-776.

458   Zhu, Y. and X. Liang (2020). "Coupling of the Surface and Near-Bottom Currents in the Gulf of Mexico." J Geophys

459   Res Oceans **125**(11): e2020JC016488.

460   Zhu, Y., J. Sun, Y. Wang, Z. Wei, D. Yang and T. Qu (2017). "Effect of potential vorticity flux on the circulation in

461   the South China Sea." Journal of Geophysical Research: Oceans **122**(8): 6454-6469.

462   Zhu, Y., Sun, J., Wang, Y., Li, S., Xu, T., Wei, Z. and Qu, T., 2019. Overview of the multi-layer circulation in the

463   South China Sea. Progress in Oceanography, 175, pp.171-182.

464   Zhou, C., Xiao, X., Zhao, W. et al. Increasing deep-water overflow from the Pacific into the South China Sea revealed

465   by mooring observations. Nat Commun 14, 2013 (2023). https://doi.org/10.1038/s41467-023-37767-4

466

467